THE EMBEDDED GRID-CONCEPT AND TSP METHODS APPLIED TO THE CALCULATION OF TRANSONIC FLOW ABOUT WING/BODY/NACELLE/PYLON-CONFIGURATIONS

ICAS-88-4.7.2

Wang Dieqian
Northwestern Polytechnical University, Xi'an, The People's Republic of China
and
Sven G. Hedman
The Aeronautical Research Institute of Sweden (FFA), Box 11021, S-161 11 BROMMA, Sweden

Abstract

A local cylindrical grid is embedded in a global Cartesian grid. The two grids overlap slightly in a narrow common zone, where the two potential fields communicate. Boundary conditions at nacelle and pylon surfaces are prescribed in the cylindrical system, and at wing and body surfaces in the Cartesian one. At the common zone potential values from one system are given as boundary values for the other system.

The potential equation for the wing/body-system was derived under the assumption that all the disturbance velocities would be small, while to model the flow at the nacelle the equation for the nacelle/pylon-system permits large disturbances in the longitudinal direction.

Pressure distributions have been computed and compared with experimental data for a configuration resembling a modern commercial airliner at Mach numbers 0.30 and 0.75. It was found that the method succesfully predicted the essential features of the flow.

Nomenclature

Variables

a	speed of sound
C_A	mass flux ratio
C_p	pressure coefficient
M	Mach number
$\bar{n}$	surface normal
R	body radius
V	total velocity
V_∞	free stream velocity
x,r,θ	cylindrical coordinate system
x,y,z	Cartesian coordinate system
α	angle of attack
γ	specific heat ratio
δ	parameter
ε	scaling parameter
η	relative span coordinate
ν	inverse jet velocity ratio
ρ	density
τ	wing thickness ratio
Φ	velocity potential
ϕ	disturbance velocity potential

Subscripts

1,2	indices
i,j,k	mesh indices
e	exit
J	jet
∞	infinity
x,r,θ	partial derivatives
x,y,z	partial derivatives

Copyright © 1988 by ICAS and AIAA. All rights reserved.

I. Introduction

The transonic speed regime is of extreme importance, since it is in this speed range that most civil aircraft cruise and most military airplanes maneuver. Because of the mixed character of the flow the prediction of load is difficult. Thus, there is a need for further development of numerical methods for transonic flow over complete configurations.

In practical aircraft design there is a need for repeated numerical calculations using cost-effective methods. TSP methods based on proper consideration of the order of magnitude of physical and mathematical terms give valuable insight into the nature of transonic flow.

The Cartesian grid used for calculation of wing/body-flow is not well suited for a nearly axisymmetrical nacelle. Instead an embedded cylindrical grid is here chosen for the nacelle/pylon-flow calculation. In planes normal to the oncoming flow direction the two grids overlap each other. Potential values in one grid are interpolated to boundary points of the other grid to serve as boundary values for the solution. Iterations are then performed alternatively in the two grids.

The jet flow from a working engine is modelled with a scaled potential. The pressure is made continuous through the jet boundary.

II. Wing/Body-Flow Method

Potential Equation

A disturbance potential ϕ is defined from the full velocity potential Φ[1],

$$\Phi(x,y,z)= V_\infty[x+\varepsilon\ \phi(x,y,z)]$$

with $\varepsilon=\tau^{2/3}/M_\infty$, a scaling parameter. With the assumption that all three disturbance velocity components are small, the transonic small perturbation equation may be written

$$\{(1-M_\infty^2)-[3-(2-\gamma)M_\infty^2]M_\infty^2\varepsilon\ \phi_x\}\phi_{xx} + \phi_{yy}+\phi_{zz}= 0 \qquad (1)$$

The equation is transformed into finite difference form and solved by successive line over relaxation.

A consistent pressure coefficient relation has been used

$$C_p=\{-2\ \varepsilon\phi_x- \varepsilon^2[(1-M_\infty^2)\phi_x^2+\phi_y^2+\phi_z^2] + \varepsilon^3[3-(2-\gamma)M_\infty^2]\ M_\infty^2\ \phi_x^3/3\}$$

Boundary Conditions

The boundary condition of no mass flux through the surface, using the same assumption as for (1), is

$$\left(\frac{\rho}{\rho_\infty}\frac{\overline{V}}{V_\infty}\right)\cdot\overline{n} = 0$$

$$\phi_z=\left\{\frac{1}{\varepsilon}+(1-M_\infty^2)\phi_x-\frac{1}{2}\left[3-(2-\gamma)M_\infty^2\right]M_\infty^2\ \varepsilon\ \phi_x^2\right\}f_x + \phi_y\ f_y$$

where $z=f(x,y)$ describes the wing surface.

For grid points representing the body the velocity vector is put parallel to the configuration surface and the boundary condition is given by

$$\phi_z=\left(\frac{1}{\varepsilon}+\phi_x\right)f_x+\phi_y\ f_y$$

The potential for the three streamwise farfield surfaces is estimated from expressions derived by Klunker.

At grid planes situated in the zone common to both the wing/body-grid and the nacelle grid the nacelle/pylon-potential is enforced as boundary values on the wing/body-solution.

III. Nacelle Flow Method

Potential Equation

With the assumption that the transverse velocity components were much smaller than the free stream velocity, but without corresponding restriction on the longitudinal disturbance velocity a potential equation permitting transonic flow with stagnation point was derived

$$(1-M^2)\phi_{xx}+\phi_{rr}+\frac{1}{r}\phi_r+\frac{1}{r^2}\phi_{\Theta\Theta}=0 \qquad (2)$$

$$M^2=(1+2\delta)\ M_\infty^2/\left[1-(\gamma-1)\delta\ M_\infty^2\right];\ \delta=\left(1+\frac{1}{2}\phi_x\right)\phi_x$$

Here the disturbance potential ϕ is defined

$$\Phi(x,r,\theta)=V_\infty\left[\cos\alpha\ x+\sin\alpha\ \cos\theta\ r+\phi(x,r,\theta)\right]$$

Note that for $\phi_x=-1$, M equals zero, and for $\phi_x=0$, $M=M_\infty$, and that no limitation has been imposed on the free stream Mach number.

The potential is computed by successive line over relaxation with lines in radial direction. As the equation permits large longitudinal disturbances, grid points are positioned at the contour in the leading edge region.

Pressure coefficients are computed using the exact expression.

Surface Boundary Conditions

At the nacelle surface the mass flux vector is parallel to the surface

$$\left(\frac{\rho}{\rho_\infty}\frac{\overline{V}}{V_\infty}\right)\cdot\overline{n} = 0$$

At the leading edge point where $|\phi_x|=O(V_\infty)$ the boundary condition becomes

$$\cos\alpha+\phi_x=0$$

and for the rest of the points at the contour

$$\left\{\cos\alpha+(1-M_\infty^2\cos^2\alpha)\phi_x-\frac{1}{2}\cos\alpha\left[3-(2-\gamma)M_\infty^2\cos^2\alpha\right]M_\infty^2\ \phi_x^2\right\}R_x- \qquad (3)$$
$$(\sin\alpha\ \cos\Theta+\phi_r)+(-\sin\alpha\ \sin\theta+\phi_\Theta/R)\ R_\Theta/R=0$$

where the body radius R is

$$R = R(x,\ \theta)$$

As the boundary conditions will be applied at the contour close to the lip and at points in the vicinity of the contour further away from the lip, it is an advantage to express the boundary conditions in terms of the tangential velocities, obtained through directional differentiation as is detailed in[1].

It has been found that a transonic flow is most sensitive to errors in the conservation of mass equation. So this mass flux condition used here improves the pressure distribution accuracy and convergence as well.

The boundary condition at the pylon surfaces is formulated as a velocity tangency condition.

The Kutta condition is applied at the pylon wake. The potential jump across the pylon wake is kept constant in points downstream of the trailing edge and the flow angles at the wake outboard and inboard sides, respectively, are put equal.

Intake Flow

For a nacelle the flow inside the whole length can be calculated. However, for a powered nacelle the total pressure and temperature are not the same in front of and behind the engine, and the jet and the nacelle inside have to be calculated separately.

At some control station inside the air intake a velocity distribution is given with values either from measurements or from an estimate by one dimensional flow theory with given M_∞, mass flux ratio C_A and geometry. If the exit area A_e is used as reference area for C_A, then

$$C_A=\frac{\rho_e}{\rho_\infty}\frac{V_e}{V_\infty}$$

Numerical calculation shows that internal flow away from the intake lip quickly becomes semi-one-dimensional.

The flow upstream of the control station is computed in the same way as other nacelle flow regions.

Exit Flow

To simulate the jet flow a potential flow model has been put together, which is based on the assumptions that there is no mass flux ratio change at the passage of the engine, because the mass of the added fuel is small compared to the mass of the air, that the static pressure across the nacelle exit plane equals the ambient pressure, that the main flow and jet flow can be described with the potentials Φ and Φ_J with equal static pressure at the inner and the outer side of the nacelle wake surface, and that ϕ_r, α, $\phi_\theta/R \ll \phi_x$ at the wake.

The model is derived in detail in[2].

A jet disturbance potential ϕ_J is defined, based on the jet velocity V_J.

$$\Phi_J(x,r,\theta) = V_J[x+\phi_J(x,r,\theta)]$$

ϕ_J should obey an equation similar to (2), this can be obtained if

$$\phi_J = V_\infty/V_J \ \phi$$

that is

$$\Phi_J(x,r,\theta) = V_J \ x + V_\infty \ \phi(x,r,\theta)$$

Then for the jet

$$(1-M^2)\phi_{xx} + \phi_{rr} + \frac{1}{r}\phi_r + \frac{1}{r^2}\phi_{\theta\theta} = 0$$

$$M^2 = (1+2\delta_J)M_J^2/[1-(\gamma-1)\delta_J \ M_J^2]$$
$$M_J = V_J/a_J$$
$$\delta_J = (1+1/2 \ \nu \ \phi_x)\nu \ \phi_x$$
$$\nu = V_\infty/V_J$$

If the subscripts 1 and 2 denote the inner and the outer sheet of the wake, respectively, then the equal wake static pressure condition becomes

$$\phi_2 - C_A\phi_1 = \phi_{2_{te}} - C_A\phi_{1_{te}} + \frac{1}{2}[C_A \nu \int_{x_{te}}^{x} \phi_{x_1}^2 dx - \int_{x_{te}}^{x} \phi_{x_2}^2 dx]$$

with index te for nacelle trailing edge stations.

IV. Application

An earlier program version was used for calculations on the Lockheed C5 configuration, Ref. 1. Here the present program will be applied to a modern commercial airplane configuration for which experimental pressure data have been provided by the MBB Co.[3].

Configuration

The main dimensions appear in Fig. 1. The configuration is representative of a modern airliner with a large diameter nacelle situated forward of the wing leading edge and rather close under the wing plane. In the experiments there was a central plug in the exit of the nacelle. This plug was not modelled in the calculations, instead the nacelle was extended downstream and closed to have an exit area equal to the open area at the experiments.

Grids

The nacelle/pylon grid is a cylindrical grid consisting of 72×20×17 grid points in the x,r,θ directions, respectively. Fig. 2 shows that part of a plane θ=const. which is closest to the nacelle.

For the wing/body two grids were used, a coarse grid with 60×38×46 points in the x,y,z directions, respectively, and a fine grid with 92×61×50 points. A vertical view with a part of the fine grid and the configuration appears in Fig. 3, and a view from the front of the Cartesian grid with the embedded cylindrical grid is shown in Fig. 4.

The upstream and downstream farfield planes of the two grids coincide. The farfield of the Cartesian grid is approximately ten wing halfspans away from the airplane.

Calculations

A VAX 8530 computer was used. The calculations were performed in a Cartesian wing/body-grid and in a cylindrical nacelle/pylon-grid. The strategy was, to make two iterations in one grid and then update the potential of the other at the common border. The solution for a flow case would be iterated until the maximum potential difference between two iterations had been reduced by two to three orders of magnitude. The maxima would then generally be situated at the downstream farfield, and the surface pressure distributions had stabilized. For this level of convergence some 400 iterations in the coarse wing-grid and the nacelle grid and than about 150 more iterations in the fine wing grid and the nacelle grid were run. This required about 7 CPU hours.

Results

To minimize the detrimental aerodynamic effects of the powerplant installation, the nacelle is mounted ahead of the wing leading edge, and it is connected to the wing with a slender pylon. The interference between the components is thus rather small in a well-designed installation, and no drastic pressure changes due to added components should be expected for a configuration like this.

The pressure distributions presented here were obtained at stations given in the Table.

Wing Pressures in Fine Grid

M = 0.30

η(theory):	0.139,	0.257,	0.422,	0.658
η(exp):	0.150,	0.250,	0.415,	0.650

M = 0.75

η(theory):	0.139,	0.257,	0.493,	0.658
η(exp):	0.150,	0.250,	0.500,	0.650

Wing Pressures in Coarse Grid

η(theory):	0.326,	0.419
η(exp):	0.330,	0.415

Nacelle Pressures

θ(theory):	-90.0,	-22.5,	22.5,	90.0
θ(exp):	-90.0,	-30.0,	30.0,	90.0

Pylon Pressures

z(theory): -0.40

The calculated pressure distributions have been visualized through straight lines between calculated points. This is a reasonable representation except between the first two points on the wing's upper surface, therefore a dashed line is used in this interval.

The wing's pressure distributions in Fig. 5 for Mach number 0.30 were calculated to slightly more negative values than what was obtained from the experiments at all spanwise positions. To resolve the pressure peak at the leading edge would require a still finer grid. For the higher Mach number, M=0.75, Fig. 6 shows that the lower surface pressures are in good agreement, while for the upper surface theory still predicts pressures that are too negative.

The nacelle pressure distributions at Mach numbers 0.30 and 0.75 in the Figs. 7 and 8 show good agreement between calculation and experiment. The distributions at the two Mach numbers are rather similar. The variation in circumferential direction is small, probably because the intake is far upstream from the wing, but the predicted variation agrees well with the measured one.

The pylon pressure distribution in Fig. 9 shows a peak at the pylon leading edge region and the dominating influence of the wing on the pressure.

Figs. 10 to 13 contain the influence from the nacelle/pylon positioned at η= 0.353 on the pressure at two neighbouring wing sections from coarse grid calculation and from experiments. For the forward portion of the lower surface both calculations and experiments predict lower pressures for the complete configuration than for the wing/body-combination. Towards the trailing edge of the lower side the experiments indicate very little pressure difference between the two configurations, while there is a considerable difference between the calculated pressures. Maybe the reason for this difference could be found in the simple jet model used for the calculations without any influence of viscosity.

Figs. 14 and 15 show for the two Mach numbers the calculated nacelle pressures for nacelle alone and for the total configuration. Shown are also the measured nacelle pressures for the complete configuration. The calculated influence from wing, body and pylon changes the nacelle alone curves into reasonable agreement with the experiments.

The influence of jet velocity was investigated for Mach number 0.3 with the nacelle grid embedded in the coarse wing/body-grid. The influence of an increased jet velocity can be seen from Fig. 16 to be very small and to give a small reduction in lift. The spanwise distribution of the normal force ratio, which is the normal force per unit length for the whole configuration in terms of the normal force per unit length for the wing/body-combination is shown in Fig. 17. The results seem plausible.

V. Conclusions

For the calculation of transonic flow over powered airplanes a procedure based on transonic small perturbation assumptions has been developed to compute the flow about the configurations with wing and body in a Cartesian grid and nacelle and pylon in an embedded cylindrical grid.

The procedure has been applied to a configuration resembling a modern airliner at Mach numbers 0.30 and 0.75. The results have been compared with experimental data and it was found that the method successfully predicted the essential features of the flow.

VI. References

(1) Hedman, S.G., Wang, Dieqian.: "Calculations of transonic flow about wing/body/nacelle/pylon-combinations using TSP-methods". FFA TN 1986-45.

(2) Wang, Dieqian.: "Nacelle exit flow model for TSP calculations". FFA TN 1988-20.

(3) Dziomba, B., et al, MBB, Co. "Private communications".

Acknowledgements

This work was sponsored by the Swedish Board of Technical Development (STU) and by the Chinese Aeronautical Establishment.

The geometry and the experimental data for the test case were obtained from the Messerschmitt-Bölkow-Blohm GmbH, Bremen.

The assistance through discussions with collegues at FFA and MBB is acknowledged.

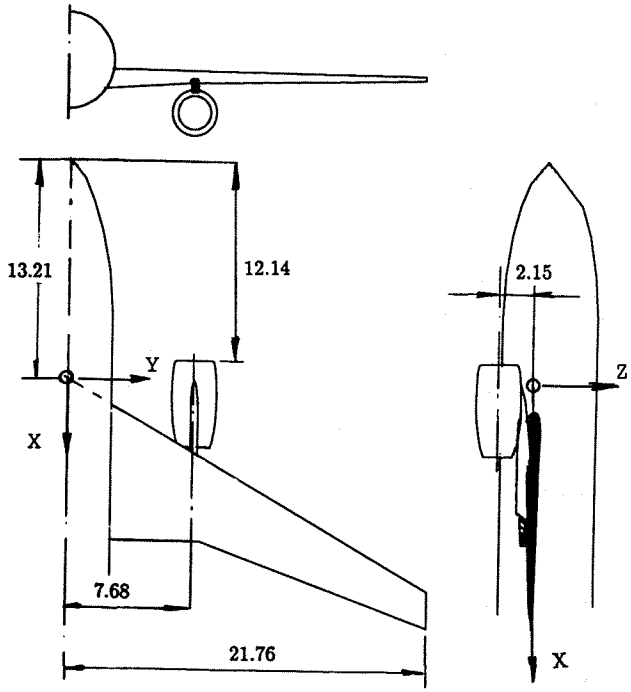

Fig. 1 Investigated configuration

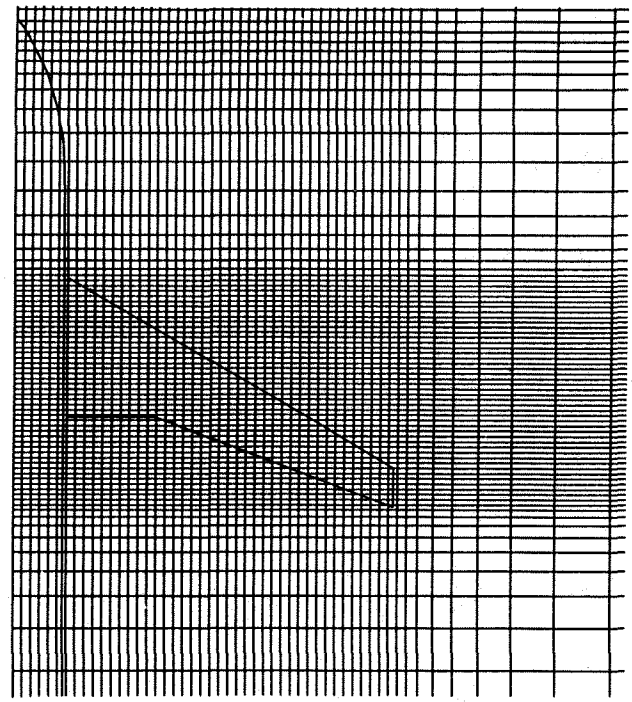

Fig. 3 Cartesian wing/body grid

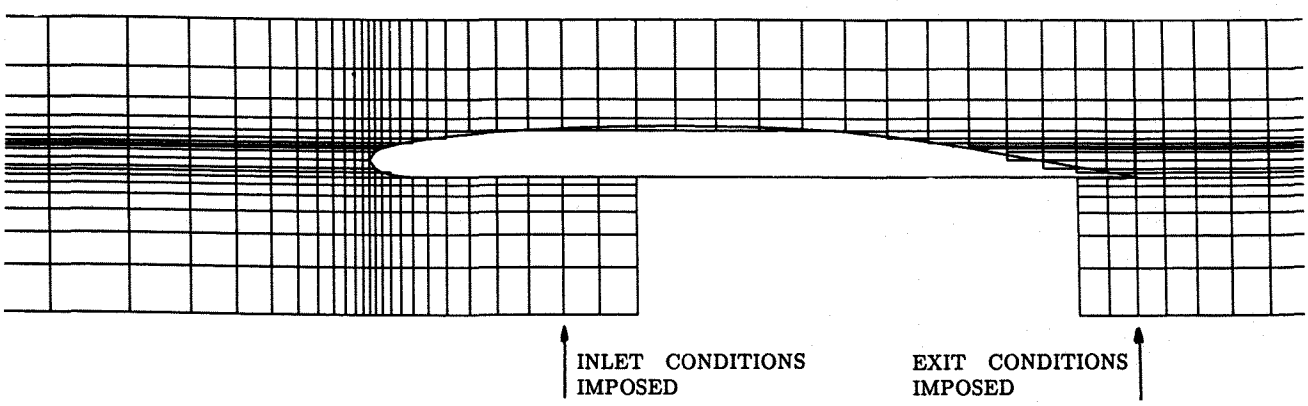

Fig. 2 Cylindrical nacelle grid θ=const plane

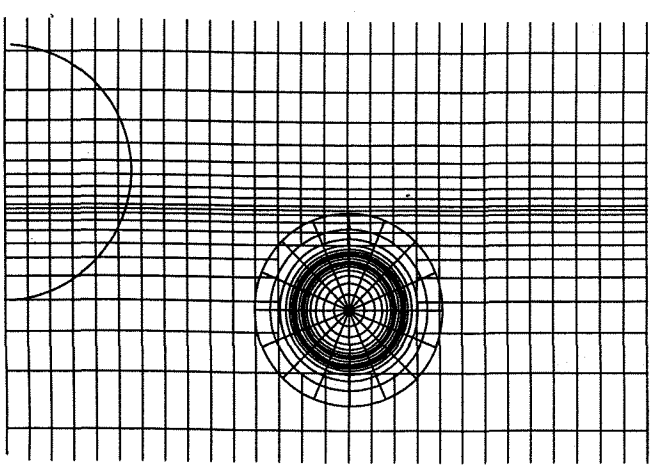

Fig. 4

Cartesian wing/body grid with embedded cylindrical nacelle grid x=const plane

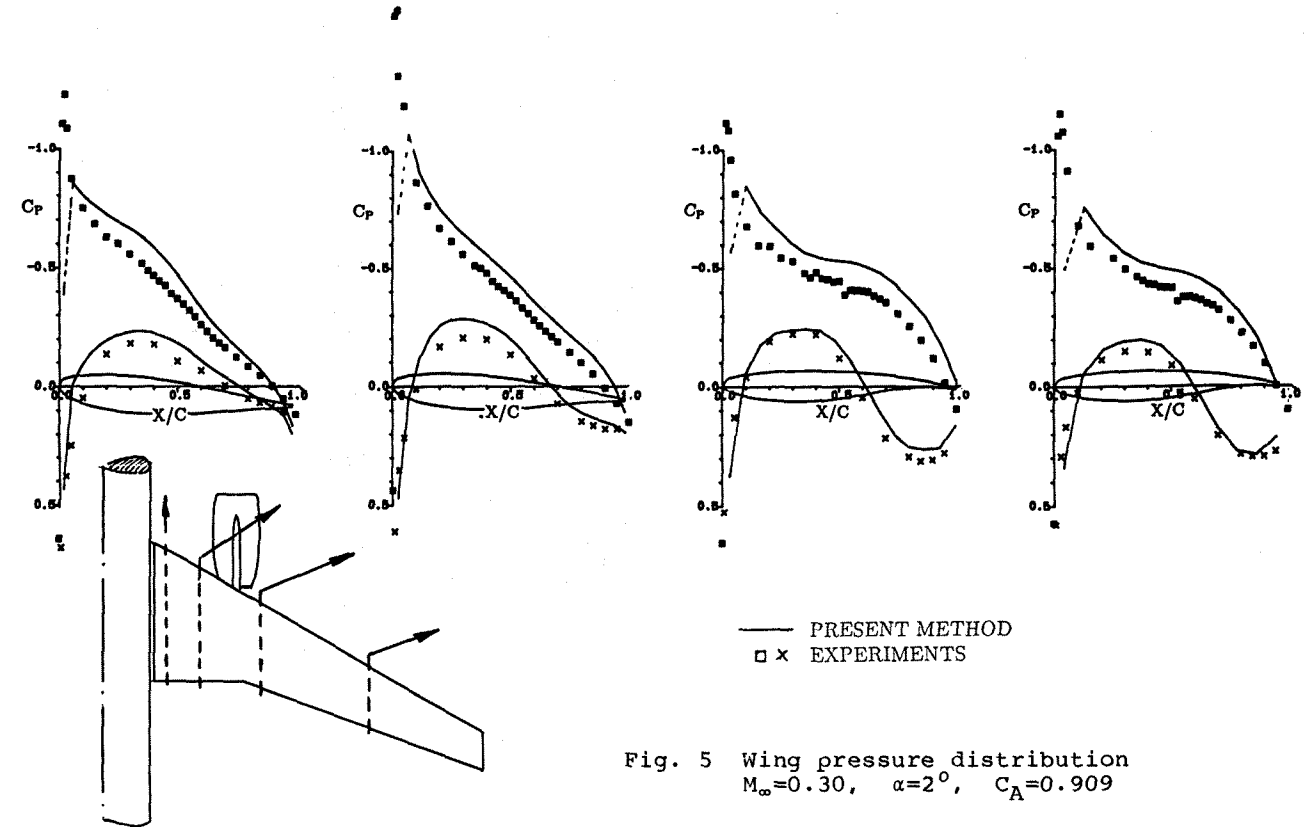

Fig. 5 Wing pressure distribution
M_∞=0.30, α=2°, C_A=0.909

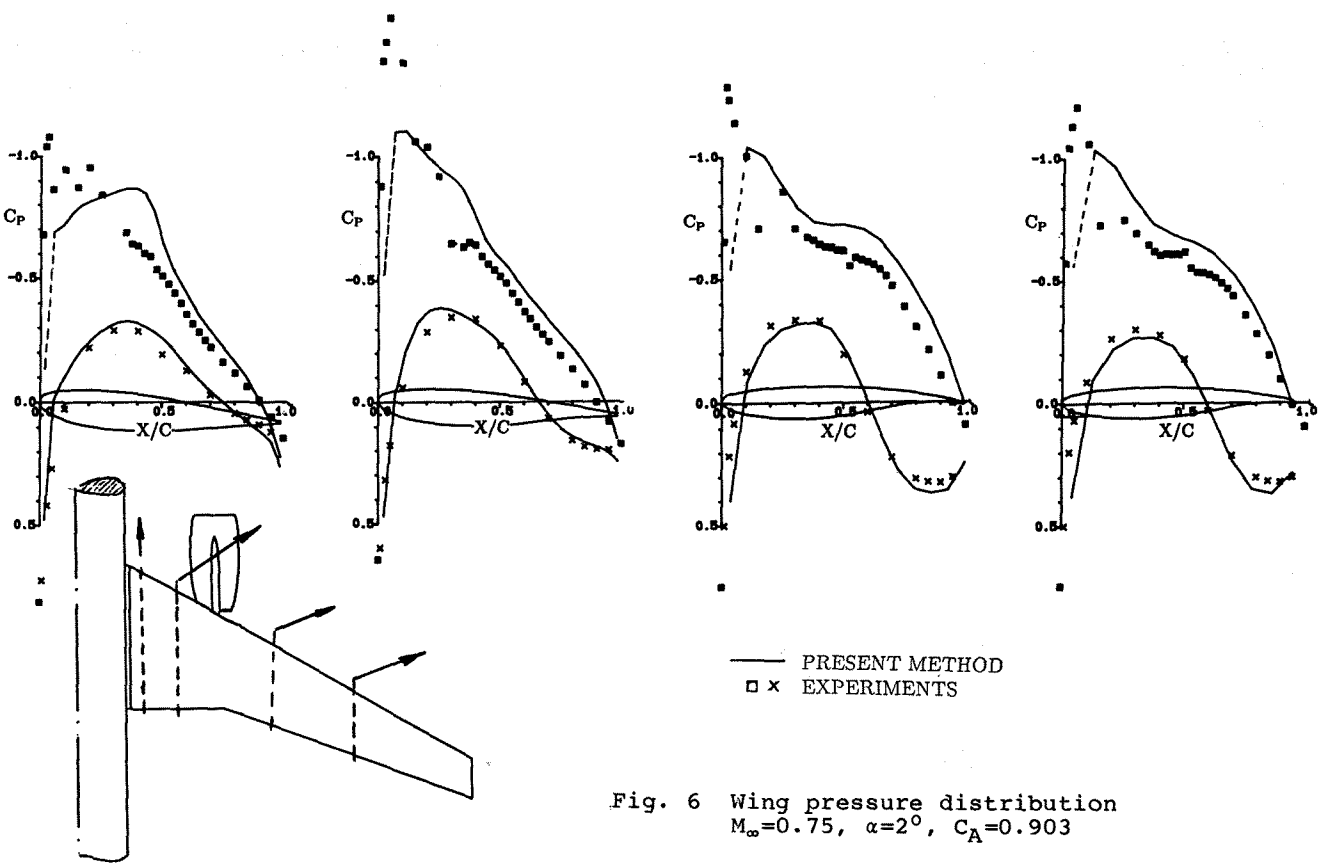

Fig. 6 Wing pressure distribution
M_∞=0.75, α=2°, C_A=0.903

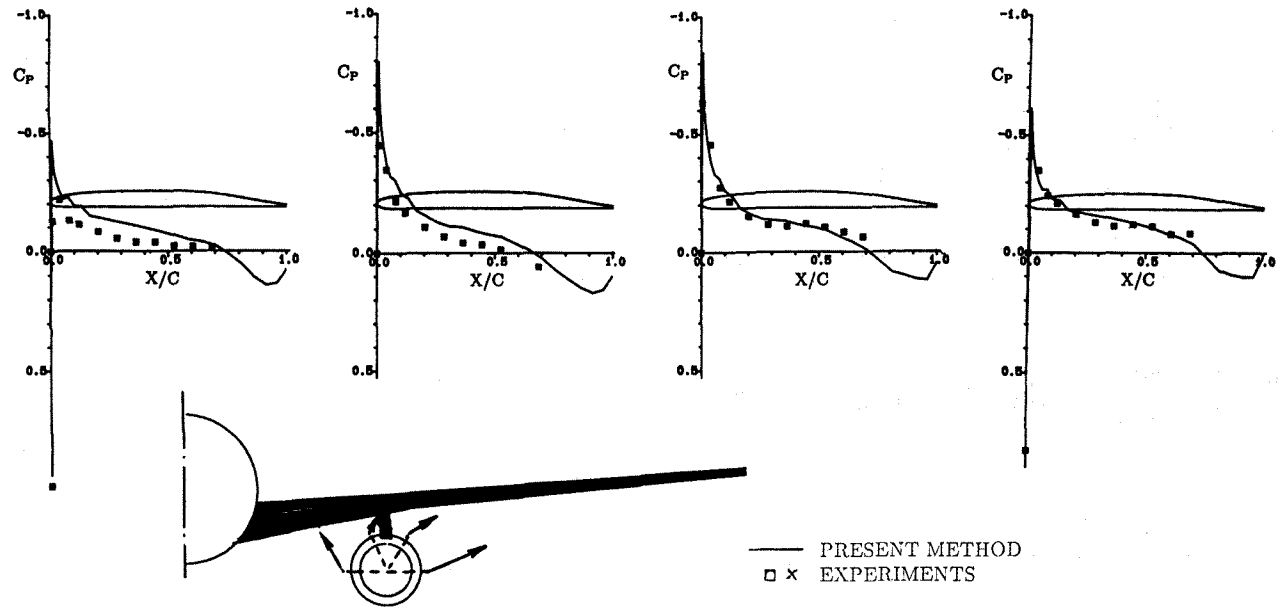

Fig. 7 Nacelle pressure distribution
$M_\infty=0.30$, $\alpha=2^o$, $C_A=0.909$

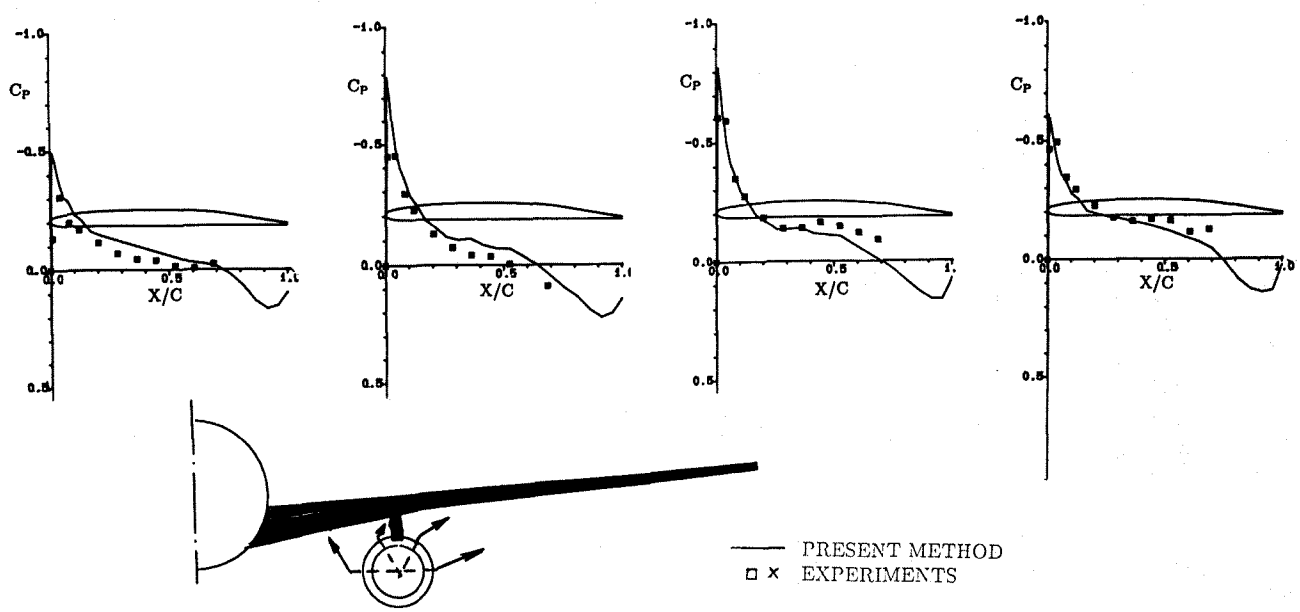

Fig. 8 Nacelle pressure distribution
$M_\infty=0.75$, $\alpha=2^o$, $C_A=0.903$

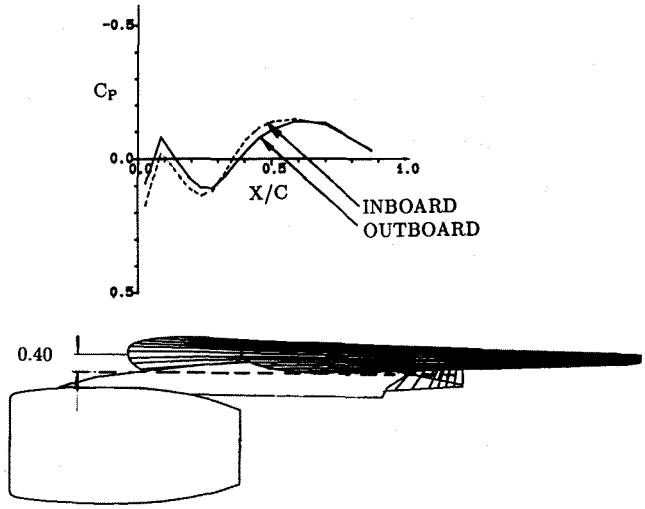

Fig. 9 Pylon pressure distribution
M_∞=0.75, α=2°, C_A=0.903

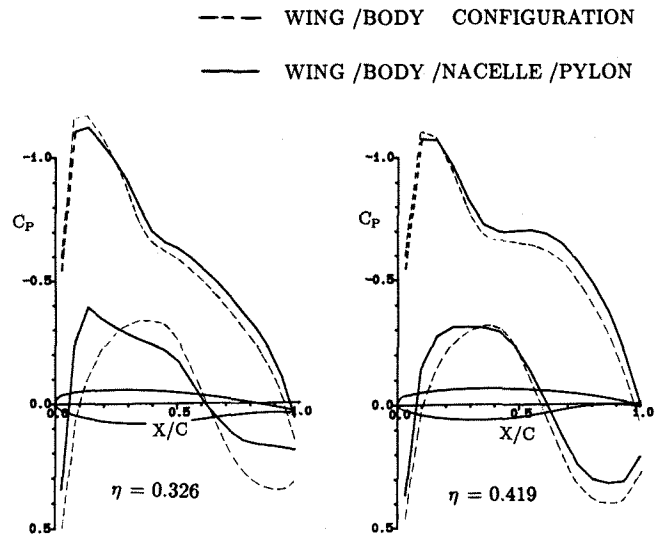

Fig. 11 Wing pressure distribution
Effect from nacelle/pylon
Theoretical results
M_∞=0.75, α=2°, C_A=0.903

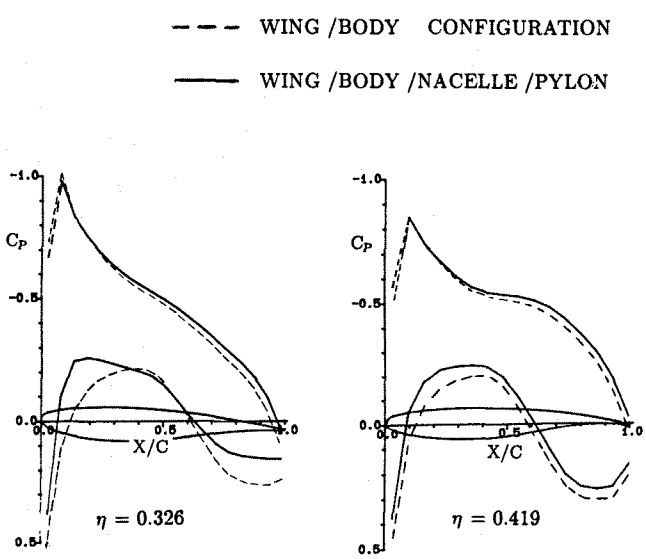

Fig. 10 Wing pressure distribution
Effect from nacelle/pylon
Theoretical results
M_∞=0.30, α=2°, C_A=0.909

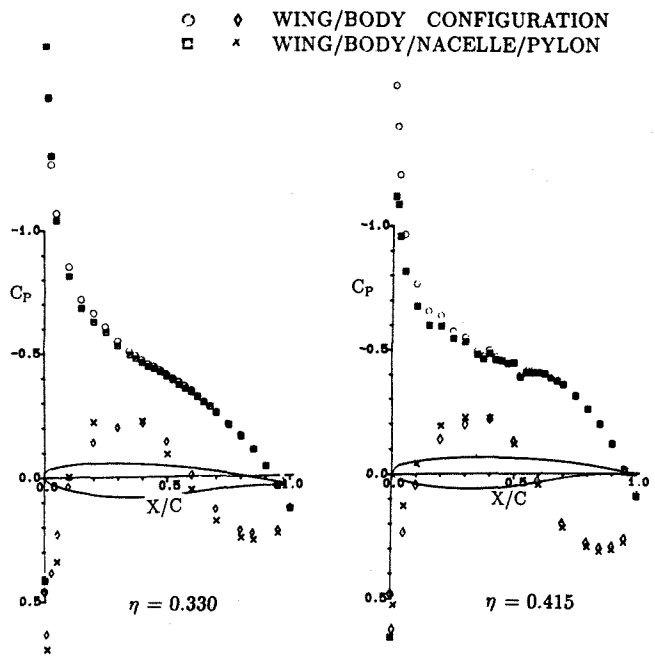

Fig. 12 Wing pressure distribution
Effect from nacelle/pylon
Experimental results
M_∞=0.30, α=2°, C_A=0.909

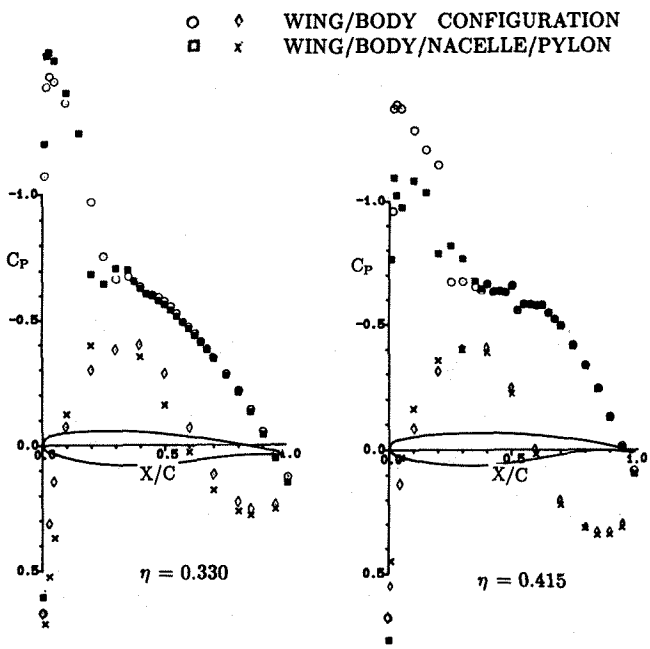

Fig. 13 Wing pressure distribution
Effect from nacelle/pylon
Experimental results
M_∞=0.75, α=2°, C_A=0.903

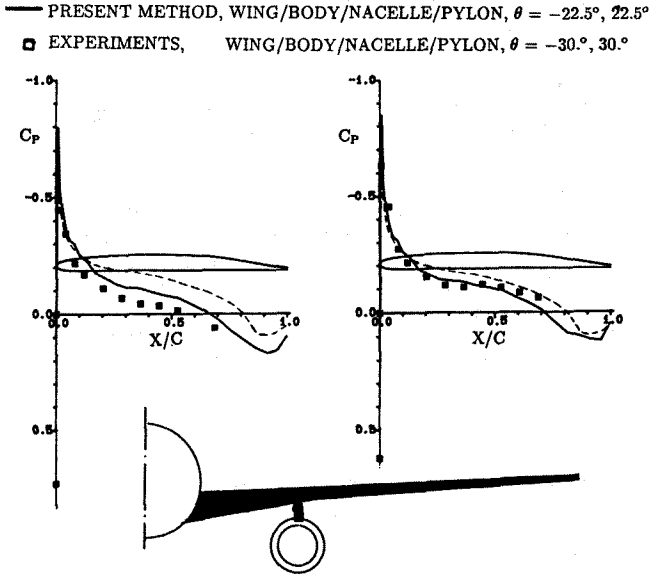

Fig. 14 Nacelle pressure distribution
Effect from wing/body/pylon
M_∞=0.30, α=2°, C_A=0.909

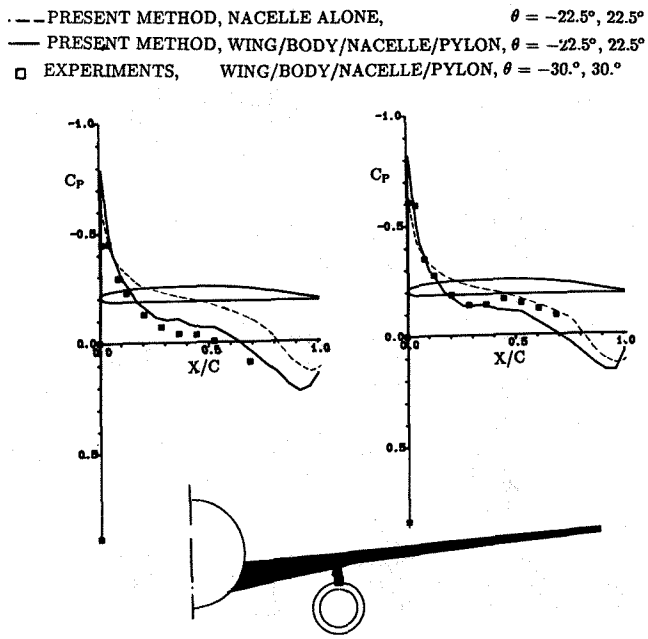

Fig. 15 Nacelle pressure distribution
Effect from wing/body/pylon
M_∞=0.75, α=2°, C_A=0.903

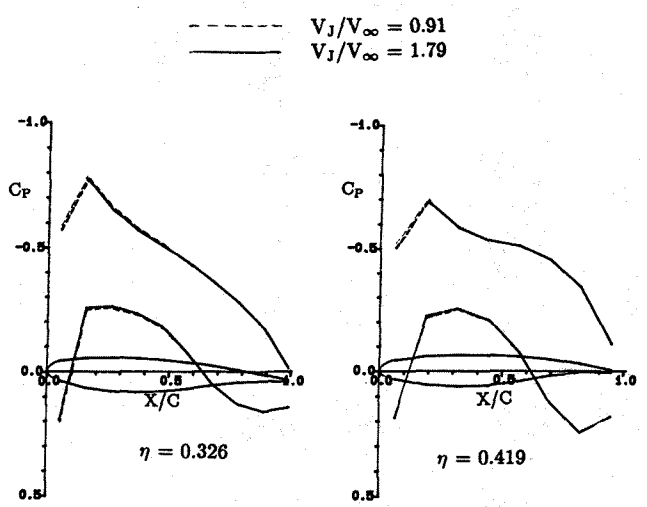

Fig. 16 Wing pressure distribution
Influence of jet velocity
M_∞=0.30, α=2°, C_A=0.909

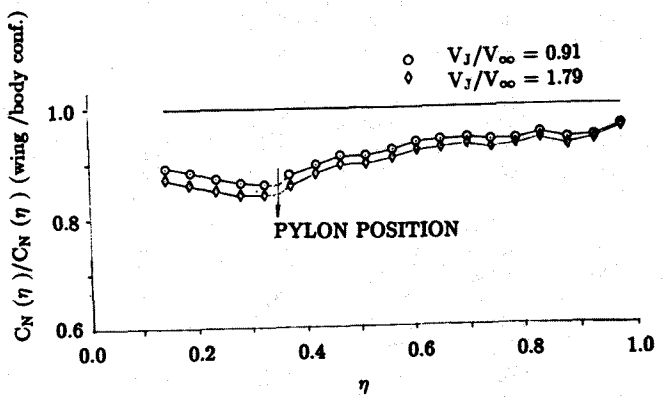

Fig. 17 Spanwise load distribution
Influence of jet velocity
M_∞=0.30, α=2°, C_A=0.909